PERGAMON

International Journal of Solids and Structures 36 (1999) 1471–1501

INTERNATIONAL JOURNAL OF SOLIDS and STRUCTURES

Effective elastic behavior of some models for 'perfect' cellular solids

Joachim L. Grenestedt*

Department of Aeronautics, Kungl Tekniska Högskolan (Royal Institute of Technology), S-100 44 Stockholm, Sweden

Received 16 August 1997; in revised form 21 January 1998

Abstract

The effective elastic behavior of some models for low density cellular solids, or solid foams, are calculated using analytical and numerical techniques. The models are 'perfect' in the sense that imperfections or irregularities as often encountered in real foams have been removed. We believe that the present models can serve as references to which more advanced models which include imperfections and irregularities can be compared. The work in this paper does not address buckling or yielding in cell walls, which play an increasingly important role as foam stresses increase. © 1998 Elsevier Science Ltd. All rights reserved.

1. Introduction

The aim of this paper is to present some presumably new models for low density cellular solids, or solid foams. A number of older models will be revisited for comparative reasons. Cellular solids have a number of applications including core material for sandwich structures, sound insulation, shock absorption, etc. Various grades of expanded PVC based foams are widely used a sandwich core materials, for example for naval composite material vessels, and PMI foams and aluminum or Nomex honeycombs for aircraft parts. Metal foams made of for example aluminum seem to have a potential to greatly outperform the polymer foams and, in some applications, also the honeycombs. The reasons include good mechanical properties when compared with the polymer foams, and good environmental properties when compared with honeycombs. Honeycombs may trap quite significant amounts of water which tend to diffuse through composite material skins, particularly in naval applications. However, at the present time, the mechanical properties of metal foams are considerably lower than what would be expected by comparing with for example PVC based foams. The difference in mechanical behavior between the metal and polymer foams can hopefully be understood by analyzing different models for cellular solids. This is done in the present paper.

* Fax: 46-8-207865; e-mail: joachim@flyg.kth.se

PII: S0020–7683(98)00048–1

Cellular solids can roughly be divided into two groups, open and closed cell materials. The open cell materials generally consist of a network of interconnected rod or beam-like members (struts), whereas closed cell materials consist of a network of interconnected plate of shell like members (walls). Occasionally, both cell struts and walls will be collectively referred to as 'cell walls' in the paper. The emphasis of the present paper is on 3-D modeling of closed cell materials. Some simple models for open cell materials are included, but these should rather be regarded as an introduction to the closed cell materials. We will presently not consider models which consist of both beam and plate or membrane elements, which, however, may be appropriate for some closed cell materials which have rather thick edges (where cell walls meet) and thin cell walls.

The paper is organized as follows: in Section 2 the concept of effective properties of cellular solids are reviewed. In Section 3, some scaling laws for cellular solids are derived by simple means. Section 4 is devoted to open cell models. Two simple models for open cell materials are presented, one consisting of a cubically symmetric periodic arrangement of struts, and the other of randomly arranged struts. These are not realistic models for open cell materials, but they provide some qualitative insight. A more realistic model, due to Warren and Kraynik (1997) is briefly discussed. In Section 5, eight closed cell models are presented. These include five analytical models: Hashin's (1962) composite spheres model, a box-like model, two models which are built of hollow spheres, and a model consisting of randomly arranged plates. Stiffnesses are presented along with these models. Three finite element (FE) models are also analyzed, one consisting of 'truncated' hollow spheres, and two consisting of flat faced polyhedra: the Kelvin foam, and an FCC arrangement with two different polyhedra. The results from the FE analyses are presented in Section 6. Section 7 summarizes some experimentally measured stiffnesses of polymer and metal foams. A note on scaling of stiffness with density is made in Section 8, and a discussion on reasons for deviations between theory and experiments in Section 9. The paper is summarized and concluded in Section 10.

2. Cellular solids: effective elastic properties, anisotropy and isotropy

This study is primarily concerned with global, or macroscopic, elastic behavior of cellular solids. If a block (or representative volume element, RVE) of cellular solid, which is large when compared to the size of single cells and cell walls, is subjected to uniform displacements on its boundaries, then the tractions on the boundaries will vary enormously on the micro level. The tractions will be zero where there is no material (where the sides of the RVE intersect the interior of a cell), and non-zero where there is material. However, on the macro level the tractions may be considered uniform save for a short wave length fluctuation about the mean traction. Macroscopic stress $\bar{\sigma}_{ij}$ and strain $\bar{\varepsilon}_{kl}$ are introduced as volume averages over an RVE. Overhead bars are used for macroscopic foam quantities, while the absence of a bar is used for a cell wall quantity (fully dense material). Macroscopic elastic stiffnesses are introduced as the quantities relating macroscopic stress $\bar{\sigma}_{ij}$ to macroscopic strain $\bar{\varepsilon}_{kl}$,

$$\bar{\sigma}_{ij} = \bar{C}_{ijkl}\bar{\varepsilon}_{kl} \Leftrightarrow \bar{\varepsilon}_{ij} = \bar{S}_{ijkl}\bar{\sigma}_{kl} \tag{1}$$

The strain energy density and the complementary strain energy density in the foam are, respectively,

$$\bar{W} = \tfrac{1}{2}\bar{C}_{ijkl}\bar{\varepsilon}_{ij}\bar{\varepsilon}_{kl}$$
$$\bar{W}^* = \tfrac{1}{2}\bar{S}_{ijkl}\bar{\sigma}_{ij}\bar{\sigma}_{kl} \tag{2}$$

Here and in the remainder of the paper, the summation convection is used, with Latin indices ranging from 1–3, and Greek indices from 1–2.

Some of the foam models are isotropic whereas others have cubic symmetry. For a cubic medium, there are three independent stiffnesses, $\bar{C}_{1111}$, $\bar{C}_{1122}$, and $\bar{C}_{1212}$ with the coordinate axes aligned with the cubic axes. A measure for the anisotropy[1] is

$$a = \frac{\bar{C}_{1111} - \bar{C}_{1122}}{2\bar{C}_{1212}}, \quad a = 1 \quad \text{for isotropy} \tag{3}$$

This quantity will be recorded for most of the models analyzed.

Many of the real foams which we wish to model are more or less isotropic, whereas some of the models are not isotropic, but have cubic symmetry. From the results from the calculations on the cubic cells models, we may create 'equivalent' isotropic media, whose stiffnesses are given by shear moduli $\bar{G}$ and bulk moduli $\bar{K}$. Upper (Voigt) bounds on these moduli can be derived, as well as other non-bounding estimates based on for example self consistent models. Lower (Reuss) bounds can be derived for a very special model, but this lower bound has little or no practical use. The lower bound stiffnesses of a cellular solid are zero (obtained with the material clustered in non-contacting regions). The procedure to obtain isotropic stiffnesses, which will be presented for some of the models, are discussed in Appendix A.

3. Scaling laws assuming simple deformations on the micro level

First in this Section, some simple scaling laws will be derived by using mainly dimensional consideration and linearity. Later in the Section, some assumptions about the deformation mechanism on the micro level will also be used.

We are here concerned with the linear elastic stiffness of the cellular solid. The stiffness of the cellular solid, such as Young's modulus $\bar{E}$, may depend on the shape of the micro structure, the size L of the micro structure (L is here an arbitrary length which scales the whole micro structure), and the elastic properties (Young's modulus E, and Poisson''s ratio v) of the cell wall material.

[1] This measure of anisotropy is constructed by comparing the stresses in the material, resulting from two different strain states. The two strain states are identical, but applied in different directions relative to the material. The strain state $\bar{\varepsilon}_{11} = \varepsilon^*$, $\bar{\varepsilon}_{22} = -\varepsilon^*$, other $\bar{\varepsilon}_{ij} = 0$ gives rise to the stresses $\bar{\sigma}_{11} = (\bar{C}_{1111} - \bar{C}_{1122})\varepsilon^*$, $\bar{\sigma}_{22} = -\bar{\sigma}_{11}$, other $\bar{\sigma}_{ij} = 0$ (when the material has cubic symmetry). The same strain state but applied in a coordinate system rotated 45° around the x_3 axis is $\bar{\varepsilon}_{12} = \varepsilon^*$, other $\bar{\varepsilon}_{ij} = 0$, and the stresses are $\bar{\sigma}_{12} = 2\bar{C}_{1212}\varepsilon^*$, other $\bar{\sigma}_{ij} = 0$, or equivalently $\bar{\sigma}'_{11} = 2\bar{C}_{1212}\varepsilon^*$, $\bar{\sigma}'_{22} = -\bar{\sigma}'_{11}$, other $\bar{\sigma}'_{ij} = 0$ measured in the 45° rotated coordinate system. The measure of anisotropy is $a = \bar{\sigma}_{11}/\bar{\sigma}'_{11} = (\bar{C}_{1111} - \bar{C}_{1122})/(2\bar{C}_{1212})$ where $\bar{\sigma}_{11}$ is the stress measured in the original coordinate system under the first strain state, and $\bar{\sigma}'_{11}$ is the stress measured in the rotated coordinate system under the second strain state; the prime denotes quantities measured in the rotated coordinate system.

From dimensional considerations it is clear that macroscopic stiffnesses of two cellular solids which are made of the same material, and whose micro structures are identical except that the size L differs, are the same.

We will now compare cellular solids which have identical micro structures, but are made of different materials. Assume that the solid materials have the same Poisson's ratios v, but different Young's moduli E and densities ρ. Dimensional considerations give that the two quotients $\bar{E}/E$ and $\bar{\rho}/\rho$ are the same for cellular solids with identical micro structures.

The general dependence of stiffnesses such as relative Young's modulus $\bar{E}/E$ on relative density $\bar{\rho}/\rho$ in cellular materials can be estimated by assuming a deformation mechanism on the micro level, i.e. in the cell walls, and using linearity and dimensional considerations. The resulting relations agree with formulas derived by for example Gibson and Ashby (1988), who used some different foam models.

Now, assume for example that the deformation mechanism in a certain open cell 3-D material is mainly bending in the cell struts (which is appropriate for example for a 2-D honeycomb micro structure as depicted in Fig. 1 when subjected to uniaxial load in the plane). The cell struts may with sufficient accuracy be modeled by beam theory, and the problem then contains the parameters force on a cell (or on a cell strut) P [ML/T^2], cell size L [L], and cell strut (beam) bending stiffness $D = EI$ [ML^3/T^2]. Dimensions of the quantities are given within brackets; M is mass, L is length, and T is time. Due to linearity (deformations are linear in load) and dimensional considerations, local deformation δ [L] will have the form

$$\delta \propto \frac{PL^3}{D} \tag{4}$$

and the Young's modulus of the cellular solid will have the form

$$\bar{E} \propto \frac{\bar{\sigma}}{\bar{\varepsilon}} \propto \frac{P/L^2}{\delta/L} \propto \frac{D}{L^4} \tag{5}$$

Now assume that the cell struts consist of beam-like members with characteristic cross sectional dimension h [L]. The cell strut bending stiffness will then have the form

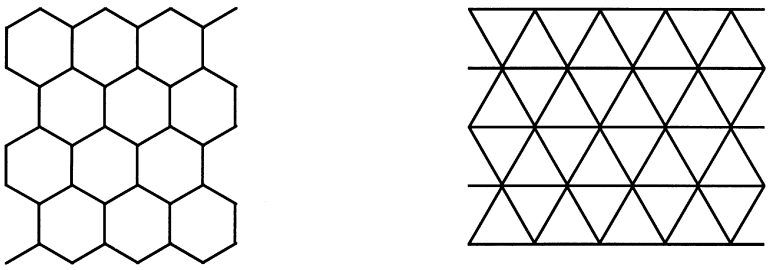

Fig. 1. Cross section of two 2-D cellular materials, honeycomb and iso-grid. The local deformation in the honeycomb (left) is bending when the in-plane effective strain is purely deviatoric. The local deformation in the iso-grid (right) is stretching. The 2-D Young's modulus $\bar{E}$ scales cubically with relative density for the honeycomb and linearly for the iso-grid, whereas bulk moduli $\bar{K}$ scale linearly for both materials.

$$D \propto Eh^4 \tag{6}$$

where E is Young's modulus of the solid material of the cells struts. The effective density is

$$\frac{\bar{\rho}}{\rho} \propto \left(\frac{h}{L}\right)^2 \tag{7}$$

assuming that the number of cell struts per unit volume foam does not change with density. In conclusion, the scaling of Young's modulus with density is

$$\bar{E} \propto E\left(\frac{h}{L}\right)^4 \propto E\left(\frac{\bar{\rho}}{\rho}\right)^2 \tag{8}$$

for an open cell bending controlled 3-D micro structure.

Similar analyses are easily performed for stretching controlled open cell materials, twisting controlled open cell 3-D materials, and bending and stretching controlled closed cell materials. The results are summarized as:

$$\bar{E} \propto E\left(\frac{\bar{\rho}}{\rho}\right)^m \tag{9}$$

where

2-D: $m = 1$ for stretching controlled micro structures
$m = 3$ for bending controlled micro structures
3-D: $m = 1$ for stretching controlled rod and plate like micro structures
$m = 2$ for bending or twisting controlled rod like micro structures
$m = 3$ for bending controlled plate like micro structures

In particular, we observe that stiffnesses scale cubically ($m = 3$) with density for closed cell bending controlled micro structures.

The procedure outlined here can be used for any stiffness. Note that different stiffnesses may scale differently with density for a given cellular solid. For example, the local deformation in a 2-D honeycomb as depicted in Fig. 1 is mainly bending when the in-plane effective strain is purely deviatoric, whereas the local deformation is stretching when the effective strain is purely dilatational. The in-plane Young's modulus and shear modulus thus scale cubically with relative density, whereas (in-plane) bulk modulus scales linearly.

4. Models for open cell foams

In this Section, three different models for open cell foams are discussed. The first model is far from physically realistic, but it does provide some results which coincide with those of other more sophisticated models.

4.1. *Stretching controlled open cell cube*

A very simple and rather non-realistic model for an open cell foam is here analyzed. Its only justification here is that it has some properties which coincide with those of some more physically realistic models. The model consists of 36 struts and 14 nodes—one node in each of the eight corners of a cube, and one node in the center of each of the six faces of the cube. Twelve of the struts are placed along the edges of the cube. Four struts are placed on each face of the cube, attached to one corner node each and all four attached to the node in the center of the face. In this model, the struts are assumed to be pin joined at the nodes, i.e. no moment is transferred between the struts. This assumption is of course not realistic for a cellular solid, but as stated some results of interest can still be obtained. The nodes are assumed to have no volume.

The structure has cubic symmetry and thus three independent stiffnesses. All struts have the same area A and Young's modulus E. The stiffnesses are

$$\bar{C}_{1111} = \frac{(1+\sqrt{2})EA}{L^2}$$

$$\bar{C}_{1122} = \bar{C}_{1212} = \frac{EA}{\sqrt{2}L^2} \tag{10}$$

with the coordinate axes aligned with the cubic axes of the material.[2] The density is

$$\frac{\bar{\rho}}{\rho} = \frac{3(1+2\sqrt{2})A}{L^2} \tag{11}$$

This foam model is not isotropic, but the anisotropy according to eqn (3) is $a \approx 1.21$. The bulk modulus of the foam is

$$\bar{K} = \frac{E}{9}\frac{\bar{\rho}}{\rho} \tag{12}$$

An upper (Voigt) bound isotropic medium can be constructed for this foam by equating the stiffness invariants of the isotropic medium with the stiffness invariants of the anisotropic medium, see Appendix A. This gives the shear modulus

$$\bar{G} = \frac{E}{15}\frac{\bar{\rho}}{\rho} \tag{13}$$

for the isotropic foam.

---

[2] Let us, without a deeper discussion, point out that $\bar{C}_{1122} = \bar{C}_{1212}$ is not a coincidence. The Cauchy result [see for example Born and Huang (1954) for a thorough discussion—the Cauchy result will not be re-derived here] states that the stiffness $\bar{C}_{ijkl}$ is symmetric in all indices ($\bar{C}_{ijkl} = \bar{C}_{ikjl}$ apart from the usual $\bar{C}_{ijkl} = \bar{C}_{jikl} = \bar{C}_{klij}$) for a crystal lattice with central forces only between the atoms, and the atoms moving as in a homogeneous medium. In the present model, the forces between nodes are central and the nodes move as in a homogeneous medium. The foam stiffness must thus be symmetric in all indices. For an isotropic medium, this leads to the Poisson ratio $\nu = 1/4$.

4.2. *Isotropic stretching controlled open cell micro structure*

Upper bound stiffnesses of an isotropic open cell foam consisting of straight or curved struts of uniform or non-uniform cross section can be constructed. These cell struts are assumed to have the same shape, but may be of different sizes. In a real foam, all cell struts naturally do not have the same shape. However, for this model we select a single cell strut shape which in some sense should be representative for all cell struts in the foam.

These bounds were derived by Grenestedt (1998), and we refer to that paper for a complete analysis. Presently, the upper bound is re-derived for the case the struts are straight, have uniform cross section, and are pinned at the ends.

The present upper bound stiffnesses are constructed in a similar way as the Voigt bound (see e.g. Appendix A). The only geometric assumption is that the cell struts are rod-like and thin compared to their lengths. No assumption about the connectivity of the struts is made. The bounds are thus applicable for example for both foams schematically depicted in Fig. 1 (save for the fact that the bounds are for 3-D materials), even though these two models are known to have very different stiffnesses. Presently, we subject the boundaries of a piece of foam to the displacements $u_i = \bar{\varepsilon}_{ij}x_j$, where $\bar{\varepsilon}_{ij}$ are given numbers. The volume averaged strains in the foam are $\bar{\varepsilon}_{ij}$. An assumed kinematic field is needed to construct the upper bound. The kinematic field which will be used is that each strut end, or node, translates as in a homogeneous medium, $u_i^{\text{node}} = \bar{\varepsilon}_{ij}x_j^{\text{node}}$ where x_j^{node} denotes the coordinates of the node. Within each strut, the kinematic fields are assumed to be that the axial strain is constant along the strut, and that the transverse strains equal Poisson's ratio times axial strain.

We will now study an arbitrary strut within the foam. The strut end displacements are $u_i^{\text{node}} = \bar{\varepsilon}_{ij}x_j^{\text{node}}$ in the global coordinate system. The relative strut end displacements are easy to express in displacements parallel and transverse to the strut, but it here suffices to note that these are linear in the foam strains $\bar{\varepsilon}_{ij}$. The strain energy W^r in an arbitrary strut (here indexed r) in the foam can then be written

$$W^r = \frac{V^r}{2} C^r_{ijkl}\bar{\varepsilon}_{ij}\bar{\varepsilon}_{kl} \tag{14}$$

where V^r is the volume of strut r, and C^r_{ijkl} are the components in the global coordinates of a stiffness tensor for strut r and defined by this relation. This stiffness tensor depends on the orientation of the strut, but not on the size of the strut. In strut fixed coordinates, these strut stiffness tensors are the same for all struts. The components of the tensor will be derived shortly.

The strain energy within an RVE with volume V^F of the foam will be the sum of the strain energy in all struts,

$$\bar{W} = \sum_{r=1}^{N} W^r = \frac{1}{2}\left(\sum_{r=1}^{N} V^r C^r_{ijkl}\right)\bar{\varepsilon}_{ij}\bar{\varepsilon}_{kl} \equiv \frac{V^F}{2}\bar{C}_{ijkl}\bar{\varepsilon}_{ij}\bar{\varepsilon}_{kl} \tag{15}$$

where $\bar{C}_{ijkl}$ is the stiffness of the foam, which is the quantity we are trying to calculate. This strain energy was obtained by an assumed kinematic field of all cell struts, and this strain energy is thus, an upper bound on the strain energy of the foam (due to the minimum of the potential energy,

which equals the strain energy when the only loading is boundary displacements). The foam stiffnesses are most easily obtained by constructing the stiffness invariants,

$$\bar{C}_{iijj} = \frac{1}{V^F}\left(\sum_{r=1}^{N} V^r C^r_{iijj}\right) = \left(\frac{1}{V^F}\sum_{r=1}^{N} V^r\right) C^r_{iijj} = \frac{\bar{\rho}}{\rho} C_{iijj}$$

$$\bar{C}_{ijij} = \frac{\bar{\rho}}{\rho} C_{ijij} \tag{16}$$

where the index 'r' was dropped since the stiffness invariants are the same for all self similar struts (and since they are invariants they are the same in all coordinate systems). It now remains to obtain the stiffness invariants C_{iijj} and C_{ijij} for a strut.

The strut stiffness tensor will be derived by aligning a strut with the global coordinates x_i, with one strut end in the center of the coordinate system and the other on the x_1 axis. The strut ends are given the displacements $u_i^{\text{node}} = \bar{\varepsilon}_{ij} x_j^{\text{node}}$, i.e. the axial strain in the strut is simply $\bar{\varepsilon}_{11}$. The strain energy in the strut is

$$W^r = \frac{V^r}{2} E \bar{\varepsilon}_{11}^2 \tag{17}$$

so an identification with eqn (14) gives the strut stiffnesses

$$C^r_{1111} = E, \quad \text{other } C^r_{ijkl} = 0 \tag{18}$$

and thus, the stiffness invariants are $C_{iijj} = C_{ijij} = E$. For an isotropic medium, the bulk modulus is $\bar{K} = \bar{C}_{iijj}/9$ and the shear modulus is $\bar{G} = (3\bar{C}_{ijij} - \bar{C}_{iijj})/30$. Thus, for the present foam,

$$\bar{K} = \frac{\bar{\rho}}{\rho}\frac{E}{9}$$

$$\bar{G} = \frac{\bar{\rho}}{\rho}\frac{E}{15} \tag{19}$$

These are both upper bound moduli of an open foam consisting of straight pinned struts. Grenestedt (1998) derived the upper bounds for an open cell foam consisting of straight beams with clamped ends, and the difference to the present bounds is negligible for low density cellular solids.

The points of interest from this model is that upper bound moduli are obtained, and that the bulk modulus is the same as for the former open cell model. Another point is that the stiffness invariants of the foam are the same as the stiffness invariants of the member from which the foam is made up, multiplied with relative density. Here, the stiffness of the member is defined through the relation

$$W^r = \tfrac{1}{2} C^r_{ijkl} \bar{\varepsilon}_{ij} \bar{\varepsilon}_{kl} \tag{20}$$

where W^r is the strain energy density in member r, whose boundaries are displaced as $u_i = \bar{\varepsilon}_{ij} x_j$. This result is quite general, and it will be used for a closed cell model later in this paper.

The results of this Section have earlier been derived by Christensen and Waals (1972) and Christensen (1986) by a different approach.

4.3. *Stiffnesses of other open cell structures*

Warren and Kraynik (1997) analyzed a 3-D open cell structure which has some similarities with the honeycomb in 2-D. Beams were placed along the edges of the Kelvin foam structure (which will be further analysed in Section 5.7). The model has cubic symmetry. The bulk modulus is the same as given in eqns (12) and (19), $\bar{K} = E(\bar{\rho}/\rho)/9$, which scales linearly with density [$m = 1$ in eqn (9)]. When subjected to dilatational deformations, the deformation mechanism in the cell struts is only stretching.

The shear stiffnesses, on the other hand, scale quadratically with density, since the cell struts deform by bending and twisting under deviatoric deformations [$m = 2$ in eqn (9)]. A number of other open cell models are discussed in the paper by Warren and Kraynik (1997), which is recommended for further details.

5. Models for closed cell foams

In the following eight Sub-Sections, eight different models for closed cell foams are discussed. The first two models are old, but the others are believed to contain some new aspects.

Gas compressibility may affect the macroscopic stiffnesses of, in particular, closed cell cellular solids. Under quasi static, hydrostatic macroscopic loads and small strains, gas compressibility increases the bulk modulus by an amount approximately equal to the gas pressure in the cells in the undeformed cellular solid. The gas pressure in the cells of most cellular solids are near atmospheric pressure, so gas compressibility may increase the bulk modulus by approximately 0.1 MPa. In the remainder of the paper, this effect is ignored.

5.1. *Multi-disperse hollow spheres model, and Hashin–Shtrikman upper bounds*

Hashin (1962) introduced a composite spheres model which has been used for obtaining properties of closed cell cellular solids. This model consists of hollow spherical shells which all have the same ratio of wall thickness to diameter, but different sizes. The spheres are arranged such that they fill space—every 'hole' between spheres is filled with smaller spheres, and so on, until space eventually is filled. Figure 2 depicts the foam, but without many of the smaller spheres.

The bulk modulus is easily calculated for this model, and it equals the Hashin–Shtrikman (1963) upper bound for a solid consisting of dense isotropic material (the material in the cell walls) and voids, where the void shape and the distribution is such that the resulting cellular solid is isotropic. The Hashin–Shtrikman bound for the bulk modulus is

$$\bar{K} = \frac{4GK(\bar{\rho}/\rho)}{4G + 3K(1-\bar{\rho}/\rho)} \underset{\bar{\rho}/\rho \to 0}{\rightarrow} \frac{\bar{\rho}}{\rho}\frac{4GK}{4G+3K} = \frac{\bar{\rho}}{\rho}\frac{2E}{9(1-\nu)} \tag{21}$$

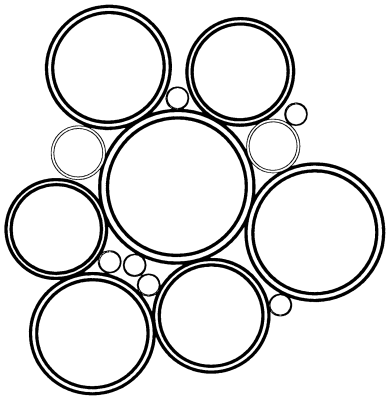

Fig. 2. Schematic of multi-disperse hollow spheres model. All space between spheres should be filled with smaller spheres, not depicted in the figure.

The low density asymptote is of particular interest for the low density foams, and it will be used to normalize results from other models below. The Hashin–Shtrikman (1963) upper bound for the shear modulus is

$$\bar{G} = \frac{G(9K+8G)(\bar{\rho}/\rho)}{15K+20G-6(K+2G)(\bar{\rho}/\rho)} \underset{\bar{\rho}/\rho \to 0}{\rightarrow} \frac{\bar{\rho}}{\rho}\frac{G(9K+8G)}{5(4G+3K)} = \frac{\bar{\rho}}{\rho}\frac{E(7-5v)}{30(1-v^2)} \tag{22}$$

The lower bounds for both $\bar{K}$ and $\bar{G}$ naturally vanish (obtained with all material clustered in non-contacting regions).

For fixed Young's modulus E of the cell wall material, $\bar{K}$ is according to eqn (21) increasing for increasing Poisson ratio v, whereas $\bar{G}$ has a minimum for $v = (7-\sqrt{24})/5 \approx 0.42$ and increases for v away from this value.

5.2. *Stretching controlled closed cell box model*

Another even simpler model of a cellular solid consists of cubic boxes arranged in a cubic lattice, or three sets of parallel planes where each set is normal to one of the three Cartesian coordinate axes. The model is depicted in Fig. 3. This model has been employed for example by Matonis (1964) to calculate critical compressive stresses of foams. The stiffnesses for a low density cellular material with this structure are

$$\begin{aligned}
\bar{C}_{1111} &= \frac{2E}{3(1-v^2)}\left(\frac{\bar{\rho}}{\rho}\right) \\
\bar{C}_{1122} &= \frac{Ev}{3(1-v^2)}\left(\frac{\bar{\rho}}{\rho}\right) \\
\bar{C}_{1212} &= \frac{G}{3}\left(\frac{\bar{\rho}}{\rho}\right)
\end{aligned} \tag{23}$$

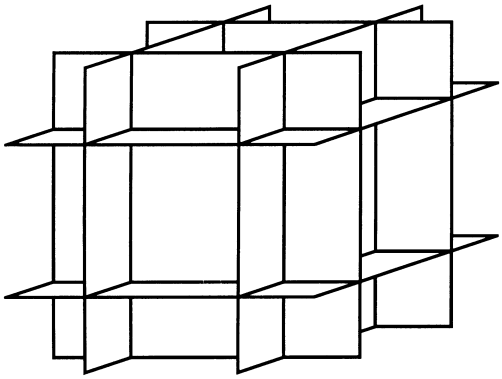

Fig. 3. Box model consisting of flat plates.

with the coordinate axes aligned with the cubic axes of the material. The bulk modulus is

$$\bar{K} = \bar{C}_{iijj}/9 = (\bar{C}_{1111} + 2\bar{C}_{1122})/3 = \frac{2E}{9(1-v)}\left(\frac{\bar{\rho}}{\rho}\right) \tag{24}$$

which equals the low density asymptote of the Hashin–Shtrikman upper bound, eqn (21).

This cell model has cubic symmetry but is not isotropic. The anisotropy is

$$a = \frac{2-v}{1-v} \tag{25}$$

and $v = 0.3$ makes $a \approx 2.4$. Because of the geometric simplicity of this model, it may be suited for studying for example the effect of 'imperfections', such as curvature of the cell walls, on effective properties.

5.3. *Analytic mono-disperse closed cell simple cubic hollow spheres model*

This model consists of hollow connected spheres in a simple cubically periodic arrangement, Fig. 4. The spheres are placed in rows parallel to the three Cartesian coordinate axes, and contacting each other along these rows. This arrangement is not isotropic. The following analysis was taken from Budiansky (1996).

The deformation of the spheres is quite local in nature when the spheres are thin walled, the contact region between the spheres is small, and the foam is subjected to any combination of stretchings parallel to the coordinate axes. The deformation can therefore with satisfactory accuracy be obtained from a spherical cap and shallow shell theory. In case the medium is subjected to shear deformation in the present coordinate axes, analysis of only a cap is in general not sufficient. Only analysis of a spherical cap is presently performed, and the stiffnesses $\bar{C}_{1111}$ and $\bar{C}_{1122}$ but not $\bar{C}_{1212}$ can then be determined. The methods to construct an isotropic medium cannot be used since all stiffnesses are not known, but the 'stretching' modulus $\bar{E}_S$ (Young's modulus in the direction of a lattice vector) and the bulk modulus can be calculated. These are closely related ($\bar{E}_S = 3\bar{K}$); only $\bar{K}$ will be given below.

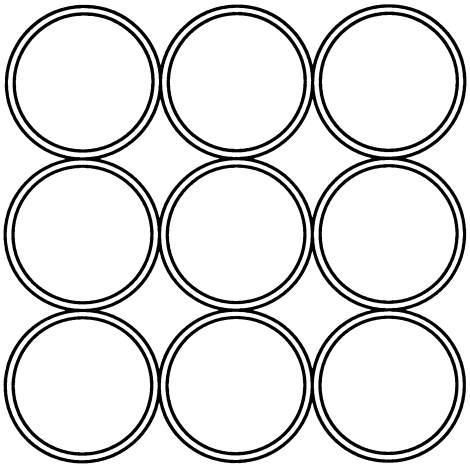

Fig. 4. Schematic of simple cubic arrangement of identical spherical shells.

The spheres will have a finite contact area which presently for simplicity is modeled as a constant pressure within a circular region (with radius r_p) corresponding to the contact regions between the spheres. The deformation state of the cap is given in Appendix B.

The bulk modulus is plotted vs relative density in Fig. 5 for different contact sizes between the spheres. Two extreme cases of the model are the case of point contact between the spheres ($\mu = 0$ in Appendix B), for which the bulk modulus is

$$\bar{K} = \frac{4E}{3\pi^2\sqrt{3(1-\nu^2)}}\left(\frac{\bar{\rho}}{\rho}\right)^2 \tag{26}$$

and $\bar{K} \approx 0.08E(\bar{\rho}/\rho)^2$ for $\nu = 0.3$. The case of vanishing relative density and finite area contact ($\mu = \infty$ in Appendix B), gives

$$\bar{K} = \frac{E}{6}\left(\frac{\bar{\rho}}{\rho}\right)\left(\frac{r_p}{R}\right)^2 \tag{27}$$

For contact regions between these two extremes, intermediate stiffnesses are obtained.

Observe that $\bar{K}$ in eqn (27) scales linearly with density when r_p/R is independent of density. $\bar{K}$ for the multi-disperse hollow spheres model, eqn (21), also scales linearly with density when the density is low, but the present $\bar{K}$ is considerably lower since $(r_p/R)^2 \ll 1$. If rather r_p/t is independent of density, then the bulk modulus in eqn (27) may be written

$$\bar{K} = \frac{2E}{3\pi^2}\left(\frac{\bar{\rho}}{\rho}\right)^3\left(\frac{r_p}{t}\right)^2 \tag{28}$$

and the scaling is cubic with density.

Equation (26) predicts that the effective bulk modulus increases with increasing Poisson ratio of the matrix material if Young's modulus of the matrix material is fixed. In eqns (27) and (28)

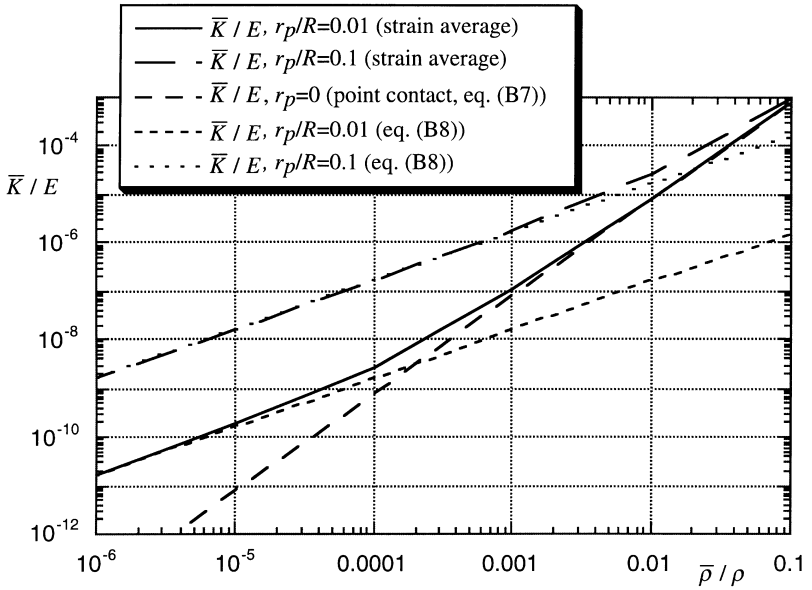

Fig. 5. Effective bulk modulus vs density of simple cubic arrangement of hollow spheres. The radius of the region of contact between spheres is 0, 1%, and 10% of the sphere radius; increasing contact radius leads to a stiffer medium. The bulk modulus was calculated by using the integrated deflection of the contact region in the strain expression. The difference to using the point values is small, see Table B1. The region of interest for practical purposes is the far right hand side.

there is no influence of Poisson ratio of the matrix material if Young's modulus of the matrix material is fixed.

It may be of interest to note that FEM calculations on this foam structure reveal that the shear stiffness $\bar{C}_{1212}$ of the cubic arrangement is very large, in fact so large that the effective Poisson ratio of an equivalent isotropic medium obtained by Voigt, Reuss, or self-consistent schemes (see Appendix A), is, at least for some materials and geometries, negative.

5.4. *Closed cell isotropic hollow spheres model*

The bulk modulus of an isotropic cellular solid consisting of hollow spheres can be approximated by assuming that each sphere is in contact with 12 other spheres. The spheres are, again, assumed to be thin walled and the contact region between the spheres small, so the approximations from the last Section apply. The arrangement of the contact points is as the centers of the sides in a regular pentagonal dodecahedron. This arrangement is isotropic, Budiansky (1987). Unfortunately it is not space filling, a fact which is presently ignored. Some geometric properties of a dodecahedron are needed. With L_0 denoting the length of an edge (where two faces meet) of a dodecahedron, and $\omega = 3\pi/10$, half the distance between two parallel opposite faces in the dodecahedron is

$$R = L_0 \tan\omega \sin\omega \tag{29}$$

The area of a pentagonal face is

$$A = \tfrac{5}{4} L_0^2 \tan\omega \tag{30}$$

and the volume is

$$V = 5L_0^3 \tan^2\omega \sin\omega \tag{31}$$

Subjecting this arrangement of spheres to hydrostatic load, the stress, strain, and relative density are, respectively,

$$\bar{\sigma}_{11} = \bar{\sigma}_{22} = \bar{\sigma}_{33} = \frac{P}{A} \tag{32}$$

$$\bar{\varepsilon}_{11} = \bar{\varepsilon}_{22} = \bar{\varepsilon}_{33} = \frac{w_0}{R} \tag{33}$$

$$\frac{\bar{\rho}}{\rho} = \frac{4\pi R^2 t}{V} \tag{34}$$

where P is the force between spheres, and w_0 is the deformation of a sphere at the point of contact with other spheres, see Appendix B. The bulk modulus for the foam is

$$\bar{K} = \frac{\bar{\sigma}_{ii}}{3\bar{\varepsilon}_{jj}} = \frac{P}{w_0}\frac{R}{3A} \tag{35}$$

which is valid also for other arrangements, such as the simple cubic arrangement discussed above. The extreme case of point contact ($\mu = 0$) gives

$$\bar{K} = \frac{5E\cos\omega}{3\pi^2 \sin^3\omega\sqrt{3(1-\nu^2)}}\left(\frac{\bar{\rho}}{\rho}\right)^2 \tag{36}$$

which should be compared with eqn (26). Here, $\nu = 0.3$ gives $\bar{K} \approx 0.1E(\bar{\rho}/\rho)^2$. The other extreme case of vanishing relative density and finite area contact, $\mu = \infty$, gives

$$\bar{K} = \frac{E}{3}\left(\frac{\bar{\rho}}{\rho}\right)\left(\frac{r_p}{R}\right)^2 \tag{37}$$

which is twice the value of eqn (27). These should also be compared with the multi-disperse hollow sphere model, eqn (21). If r_p/t is independent of density, then the bulk modulus in eqn (37) may be written

$$\bar{K} = \frac{25E\cos^2\omega}{48\pi^2 \sin^2\omega}\left(\frac{\bar{\rho}}{\rho}\right)^3\left(\frac{r_p}{t}\right)^2 \tag{38}$$

and the scaling is cubic with density; see also eqn (28).

5.5. *Isotropic stretching controlled closed cell micro structures*

Upper bounds on $\bar{G}$ and $\bar{K}$ of a system consisting of flat or wavy plates oriented in directions such that the resulting medium is isotropic can easily be derived in the same way as bounds were derived for an open cell material above; see also Grenestedt (1998). In case the cell walls are flat, the average elastic moduli of the cell walls are those of a plane stress isotropic membrane, $\sigma_{\alpha\beta} = Q_{\alpha\beta\gamma\delta}\varepsilon_{\gamma\delta}$ where

$$Q_{1111} = Q_{2222} = \frac{E}{1-v^2}, \quad Q_{1212} = G, \quad Q_{1122} = \frac{Ev}{1-v^2} \tag{39}$$

The upper bound effective moduli of the cellular solid are obtained as the Voigt bounds, i.e. by equating the invariants of the local and effective stiffness tensors and multiplying with relative density,

$$\bar{C}_{iijj} = \frac{\bar{\rho}}{\rho} Q_{\alpha\alpha\beta\beta}, \quad \bar{C}_{ijij} = \frac{\bar{\rho}}{\rho} Q_{\alpha\beta\alpha\beta} \tag{40}$$

where $\bar{C}_{iijj} = 9\bar{\lambda} + 6\bar{G}$, $\bar{C}_{ijij} = 3\bar{\lambda} + 12\bar{G}$ for an isotropic medium. Some terms have been ignored here, see Grenestedt (1998) for a discussion. The resulting foam stiffnesses are

$$\bar{E} = \frac{\bar{\rho}}{\rho} \frac{2E(7-5v)}{3(1-v)(9+5v)}, \quad \bar{v} = \frac{1+5v}{9+5v} \tag{41}$$

when the cell walls are flat. This is the highest obtainable stiffness of a low density isotropic porous solid. The bulk modulus is naturally the same as that of the box model. Both the bulk and shear moduli equal the low density asymptotes of the Hashin–Shtrikman upper bounds, eqn (21) and eqn (22),

$$\begin{aligned} \bar{K} &= \frac{\bar{\rho}}{\rho} \frac{2E}{9(1-v)} \\ \bar{G} &= \frac{\bar{\rho}}{\rho} \frac{E(7-5v)}{30(1-v^2)} \end{aligned} \tag{42}$$

5.6. *FEM model of closed cell simple cubic (SC) array of spheres with flat contact points*

A simple cubic arrangement of thin walled spheres but now with each spherical cell having large flat ends between each other, as schematically depicted in Fig. 6, were modeled using FEM. Let R denote the radius of the spherical surface, R_1 the radius of the flat cell wall between two spheres, and $L = 2\sqrt{R^2 - R_1^2}$ the length of the unit cell. The area of a spherical surface is $A_1 = 4\pi R^2(3\sqrt{1-(R_1/R)^2} - 2)$ and the area of a flat circular surface is $A_2 = \pi R_1^2$. Presently, only $R_1/L = 1/4$ was studied, for which the relative density of the cellular materials is $(\bar{\rho}/\rho) = t(A_1 + 6A_2/2)/L^3 \approx 3.27t/L$ when volume elements of order Lt^2 at intersections between cell walls are ignored. The flat circular surfaces are each shared by two unit cells and half of the wall thickness is thus allocated to each unit cell, such that in the cellular solid all cell walls have the same thickness. Periodicity and geometrically cubic symmetry were exploited together with

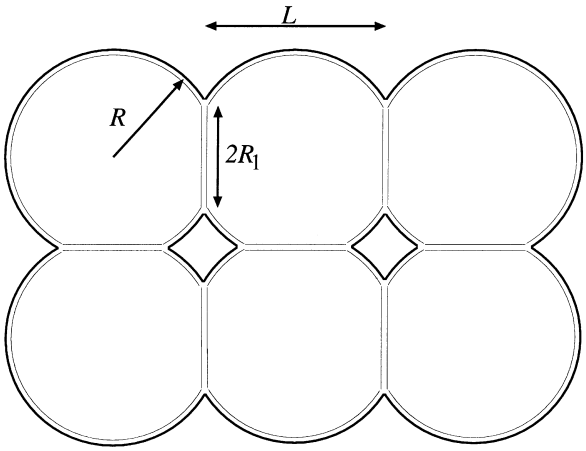

Fig. 6. Model consisting of a simple cubic array of spherical hollow shells with flat ends. The length of the unit cell is $L = 2\sqrt{R^2 - R_1^2}$.

Table 1
Elastic properties of the cellular solid using the hollow spheres SC model, with $R_1/L = 1/4$. Poisson's ratio of the matrix is $v = 0.3$. Young's moduli should be compared with the Young's moduli of the low density asymptotes of the Hashin–Shtrikman upper bounds, eqn (43), which are $\bar{E}/E = 0.00499, 0.0150, 0.0499$ for the relative densities $\bar{\rho}/\rho = 0.01, 0.03, 0.1$, respectively

$\frac{\bar{\rho}}{\rho}$	$\frac{t}{L}$	$\frac{\bar{C}_{1111}}{E}$	$\frac{\bar{C}_{1122}}{E}$	$\frac{\bar{C}_{1212}}{E}$	$\frac{9\bar{K}(\rho/\bar{\rho})}{2E/(1-v)}$ [a]	a, eqn (3)	$\frac{\bar{E}}{E}$ Voigt Self cons. Reuss	$\bar{v}$ Voigt Self cons. Reuss
0.01	0.00306	0.000961	0.000167	0.00127	0.136	0.314	0.00161 0.00147 0.00133	−0.122 −0.0683 −0.0139
0.03	0.00917	0.00348	0.000733	0.00381	0.173	0.361	0.00541 0.00501 0.00461	−0.0467 −0.00669 0.0339
0.1	0.0306	0.0163	0.00508	0.0128	0.278	0.439	0.0217 0.0205 0.0193	0.0908 0.113 0.136

[a] $\bar{K}$ is here divided by the low density asymptote of the Hashin–Shtrikman upper bound.

symmetric and anti-symmetric loadings such that only an eighth of the unit cell needed to be modeled. The calculated stiffnesses are given in Table 1. A discussion is given later, together with a discussion of the results from the FEM models presented in the next two Sub-Sections.

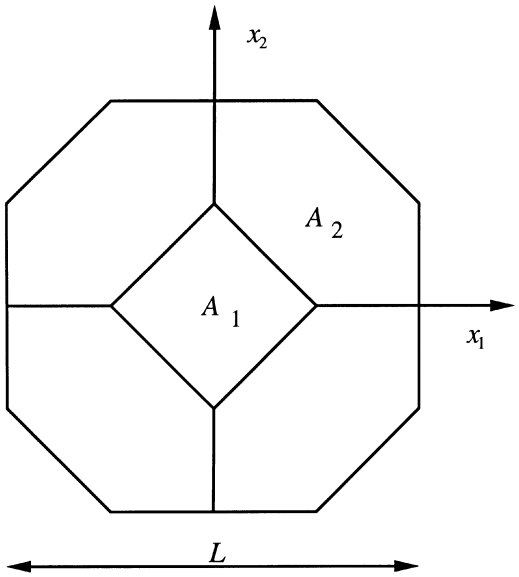

Fig. 7. A tetrakaidecahedron of the flat faced Kelvin BCC foam. The projections in the three different coordinate directions are identical. Tetrakaidecahedra of this shape can be packed in a BCC fashion and will then fill space.

5.7. *FEM model of closed cell mono-disperse Kelvin BCC polyhedral cellular solid*

Lord Kelvin (Thomson, 1887) introduced a BCC 'foam' structure[3] fulfilling Plateau's (1873) laws of a cellular foam structure in equilibrium and with surface tension and isotopic pressures as only stresses in the cell walls and isotropic pressures within the cells. The structure consists of one cell geometry, a tetrakaidecahedron with 14 faces of which six are flat with four corners and eight are slightly curved hexagons. These cells are closed and packed in a BCC arrangement. In the present analysis, the hexagonal faces were taken as flat, a simplification which seem justified by a remark by Kelvin: 'no shading could show satisfactorily the delicate curvature of the hexagonal faces'. The flat faced tetrakaidecahedron is depicted in Fig. 7. This structure is the Voronoi structure obtained from points arranged in a BCC fashion (Wigner–Seitz cell of a BCC lattice).

During the manufacturing of a cellular solid, the material is in a foam state (governed by for example surface tension and pressures) prior to solidification. The fact that Plateau's law implies that no equilibrium foam structure can consist of only flat cell walls has here been ignored. This is probably not more erroneous than to assume that the cellular solid has an equilibrium foam structure after solidification, partly due to the fact that gravity will affect the foam, and partly due to deformations occurring during solidification from the foam state. Waviness in the cell walls may be formed during solidification of a moving or vibrating liquid foam; the effect such waves have on stiffnesses has been discussed by Grenestedt (1998).

[3] For over 100 years, until Weaire and Phelan (1994) recently gave a counter-example, it was believed that this is the structure which divides space into cells with equal volume and minimum surface area.

Table 2
Elastic properties of the cellular solid using the Kelvin BCC model. Poisson's ratio of the matrix is $v = 0.3$. Young's moduli should be compared with the Young's moduli of the low density asymptotes of the Hashin–Shtrikman upper bounds, which give $\bar{E}/E = 0.00499, 0.0150, 0.0499$ for the relative densities $\bar{\rho}/\rho = 0.01, 0.03, 0.1$, respectively

$\frac{\bar{\rho}}{\rho}$	$\frac{t}{L}$	$\frac{\bar{C}_{1111}}{E}$	$\frac{\bar{C}_{1122}}{E}$	$\frac{\bar{C}_{1212}}{E}$	$\frac{9\bar{K}(\rho/\bar{\rho})}{2E/(1-v)}$	a, eqn (3)	$\frac{\bar{E}}{E}$ Voigt Reuss	$\bar{v}$ Voigt Reuss
0.01	0.00299	0.00481	0.00234	0.00134	0.998	0.922	0.00342	0.320
							0.00342	0.320
0.03	0.00896	0.0144	0.00703	0.00403	0.998	0.920	0.0103	0.319
							0.0103	0.319
0.1	0.0299	0.0484	0.0233	0.0138	0.998	0.909	0.0350	0.316
							0.0350	0.316

Table 3
Elastic properties of the cellular solid using the bi-disperse FCC model. Poisson's ratio of the matrix is $v = 0.3$. Young's moduli should be compared with the Young's moduli of the low density of the Hashin–Shtrikman upper bounds, which give $\bar{E}/E = 0.00499, 0.0150, 0.0499$ for the relative densities $\bar{\rho}/\rho = 0.01, 0.03, 0.1$, respectively

$\frac{\bar{\rho}}{\rho}$	$\frac{t}{L}$	$\frac{\bar{C}_{1111}}{E}$	$\frac{\bar{C}_{1122}}{E}$	$\frac{\bar{C}_{1212}}{E}$	$\frac{9\bar{K}(\rho/\bar{\rho})}{2E/(1-v)}$	a, eqn (3)	$\frac{\bar{E}}{E}$ Voigt Reuss	$\bar{v}$ Voigt Reuss
0.01	0.00248	0.00490	0.00226	0.00128	0.990	1.030	0.00342	0.319
							0.00342	0.319
0.03	0.00745	0.0147	0.00678	0.00386	0.990	1.029	0.0103	0.318
							0.0103	0.318
0.1	0.0248	0.0496	0.0223	0.0133	0.990	1.028	0.0352	0.313
							0.0352	0.313

The area of the flat faces in Fig. 7 are $A_1 = L^2/8$ and $A_2 = 3\sqrt{3}L^2/16$. The relative density of the highly porous solids is $(\bar{\rho}/\rho) = t(6A_1+8A_2)/L^3 \approx 3.35t/L$ where t is the thickness of the flat faces, or cell walls, L is the length of the side in the cubic calculation cell, and volume elements of order Lt^2 at intersections between faces have again been ignored. All faces in the cellular solid are assumed to have the same thickness. Faces which are shared by two calculation cells are allocated half the thickness to each cell. The presently used calculation cell consists of two tetrakaidecahedra (one body centered and eight 1/8 corner cells). Due to symmetry and periodicity, an eighth of the calculation cell is sufficient to model for mechanical analysis. The calculated stiffnesses are given in Tables 2 and 4, and a discussion is given later.

Table 4
Young's modulus and Poisson's ratio of the Kelvin BCC model as a function of Poisson's ratio of the matrix when $(\bar{\rho}/\rho) = 0.03$ ($t/L = 8.960370 \times 10^{-3}$). Young's moduli should be compared with the Young's moduli of the low density asymptotes of the Hashin–Shtrikman upper bounds, which give $\bar{E}/E = 0.0156$, 0.0150, 0.0154 for the Poisson ratios $v = 0$, 0.3, 0.45, respectively

v matrix	$\frac{\bar{C}_{1111}}{E}$	$\frac{\bar{C}_{1122}}{E}$	$\frac{\bar{C}_{1212}}{E}$	$\frac{9\bar{K}(\rho/\bar{\rho})}{2E/(1-v)}$	a, eqn (3)	$\bar{E}/E$ Voigt Reuss	$\bar{v}$ Voigt Reuss	$\bar{E}/(E(1-\bar{v}^2))$ Voigt Reuss
0	0.0131	0.00344	0.00522	0.998	0.922	0.0121 0.0121	0.197 0.197	0.0126 0.0126
0.3	0.0144	0.00703	0.00403	0.998	0.920	0.0103 0.0103	0.319 0.319	0.0115 0.0115
0.45	0.0165	0.00987	0.00363	0.997	0.918	0.00960 0.00958	0.368 0.368	0.0111 0.0111

5.8. *FEM model of closed cell bi-disperse FCC polyhedral cellular solid*

In the unit cell, this model contains four polyhedra with two different shapes. The centers of gravity of the polyhedra are arranged in an FCC fashion, but the structure is not the Voronoi structure of FCC (which consists of identical rhombic dodecahedra). One polyhedron is large and has 18 flat faces and the other three are smaller and have 12 flat faces. The large polyhedron has cubic symmetry whereas the smaller polyhedra are prolate along either Cartesian coordinate axis. The cells are depicted in Fig. 8. The foam model has cubic symmetry and thus, an eighth of the unit cell is sufficient for structural analysis. The areas of the faces of the structure are $A_1 = (3-2\sqrt{2})L^2$, $A_2 = (2-5\sqrt{2}/4)L^2$, $A_3 = (3\sqrt{2}/4-1)L^2$, where L is the length of the side in the FCC cube. In highly porous solids the relative density is $(\bar{\rho}/\rho) = t(3A_1+12A_2+12A_3)/L^3 \approx 4.03t/L$ where t is the thickness of the flat faces, and volume elements of order Lt^2 at intersections between faces in the unit cell are ignored. All faces in the cellular solid are assumed to have the same thickness, and faces shared by two unit cells are allocated half the thickness to each. The calculated stiffnesses are given in Tables 3 and 5, and a discussion is given later.

6. Results from finite element calculations on closed cell models

The general purpose finite element package ABAQUS was used for all FE analyses. All models used exclusively the shear deformable eight noded shell element S8R. There are no through-the-thickness stresses in the cell walls. Due to symmetry of the cubic unit cells, only one eighth of the cubic unit cells were modeled. Displacements were prescribed in such a way that the resulting deformation was periodic and the overall macroscopic strain state homogeneous. For determining all (cubic) elastic constants, two deformation states are sufficient if tractions are extracted and three if only strain energies are extracted from the analyses. Presently, three calculations were

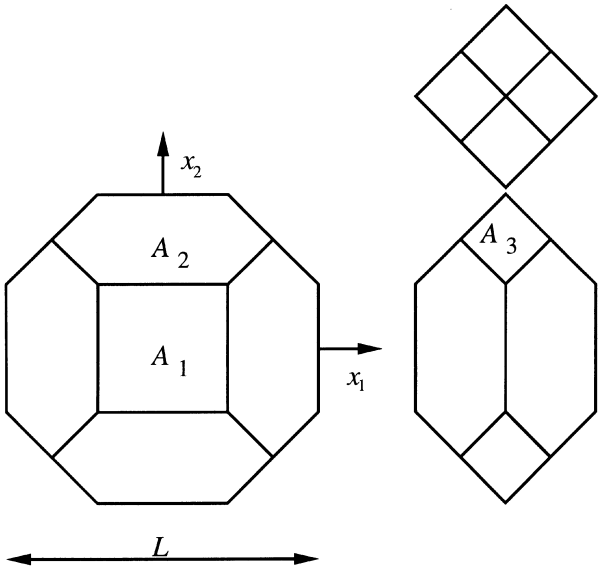

Fig. 8. Geometry of the two 'bubbles' which make up the FCC cellular solid. The left bubble has geometrically cubic symmetry.

Table 5
Young's modulus and Poisson's ratio of the bi-disperse FCC model as a function of Poisson's ratio of the matrix when $(\bar{\rho}/\rho) = 0.03$ $(t/L = 7.45 \times 10^{-3})$. Young's moduli should be compared with the Young's moduli of the low density asymptotes of the Hashin–Shtrikman upper bounds, which give $\bar{E}/E = 0.0156$, 0.0150, 0.0154 for the Poisson ratios $v = 0$, 0.3, 0.45, respectively

v matrix	$\frac{\bar{C}_{1111}}{E}$	$\frac{\bar{C}_{1122}}{E}$	$\frac{\bar{C}_{1212}}{E}$	$\frac{9\bar{K}(\rho/\bar{\rho})}{2E/(1-v)}$	a, eqn (3)	$\bar{E}/E$ Voigt Reuss	$\bar{v}$ Voigt Reuss	$\bar{E}/(E(1-\bar{v}^2))$ Voigt Reuss
0	0.0135	0.00318	0.00499	0.992	1.031	0.0121 0.0121	0.195 0.195	0.0126 0.0126
0.3	0.0147	0.00678	0.00386	0.990	1.029	0.0103 0.0103	0.318 0.318	0.0115 0.0115
0.45	0.0167	0.00960	0.00348	0.989	1.028	0.00960 0.00960	0.366 0.366	0.0111 0.0111

performed for each case (i.e., for each model, each relative density, and each Poisson ratio of the matrix), and both tractions and strain energies were extracted. Moduli determined from the tractions were slightly more consistent than those determined from strain energies, the difference most likely being due to numerical round-off errors. The two approaches are identical if the precision is exact.

For the BCC and FCC models, shown in Figs 7 and 8, the elastic anisotropy $a=(\bar{C}_{1111}-\bar{C}_{1122})/(2\bar{C}_{1212})$ is within 10% from being isotropic.[4] The BCC and FCC models are thus practically elastically isotropic. The cubic stiffnesses, as well as isotropic Young's modulus and Poisson's ratio, for the foams versus relative densities $(\bar{\rho}/\rho)$ are presented in Tables 1–5 for the SC, BCC, and FCC models. Three isotropic estimates for Young's moduli are given for each case: the Voigt, the self consistent, and the Reuss values (see Appendix A).

The Young's moduli of the three model foams, SC, BCC, and FCC, scale almost linearly with relative density. This indicates that stretching is the major deformation mechanism in these models. The ratio $(\bar{E}/E)/(\bar{\rho}/\rho)$ is then interesting to compare between the different models. The following comparison is made for the Poisson ratio of the cell wall $v=0.3$, and the data in Tables 1–3 are used. For the SC model with $R_1/L=1/4$, $(\bar{E}/E)/(\bar{\rho}/\rho)$ is between 0.13 (Reuss) and 0.16 (Voigt) for $(\bar{\rho}/\rho)=0.01$, and between 0.19 and 0.22 for $(\bar{\rho}/\rho)=0.1$. These values are the lowest of the three FE models.[5] For both the BCC and the FCC models, $(\bar{E}/E)/(\bar{\rho}/\rho)\approx 0.35$ for all densities investigated. The low density asymptotes of the Hashin–Shtrikman upper bounds on bulk and shear moduli, eqns (21) and (22), give the Young's modulus (which is an upper bound on Young's modulus since $\bar{E}$ is an increasing function of both $\bar{K}$ and $\bar{G}$)

$$\bar{E}=\frac{9\bar{K}\bar{G}}{3\bar{K}+\bar{G}}=\frac{\bar{\rho}}{\rho}\frac{2(7-5v)E}{3(1-v)(9+5v)} \tag{43}$$

For $v=0.3$, eqn (43) gives $\bar{E}\approx 0.50E(\bar{\rho}/\rho)$, which is approximately 40% higher than for the BCC and FCC models.

The bulk modulus of the SC model foam is substantially lower than the Hashin-Shtrikman upper bound. Lower densities of SC have lower bulk moduli relative to the bounds; see Table 1 where the bulk moduli have been normalized by the low density asymptote of the Hashin–Shtrikman upper bound, eqn (21). The bulk moduli of the BCC and FCC foams equal the low density asymptote of the Hashin–Shtrikman upper bound to within 1.1% for all investigated densities and Poisson ratios of the cell walls. In other words, these foam models are extremely stiff when subjected to hydrostatic loads.

The Poisson ratios of the SC model are somewhat peculiar, being negative for the lowest density $(\bar{\rho}/\rho=0.01)$. The reason has to do with the high shear stiffness of a sphere as compared to the uniaxial stiffness of the sphere.

The Poisson ratios of the BCC and FCC models are 0.31–0.32 for all densities, when $v=0.3$ for the cell walls. Divinycell (1995, 1992a, b) reports in their material manuals the Poisson ratio 0.32 for the closed cell PVC based polymer foam grades H, HT, and HCP, for all foam densities.

Cherkaev et al. (1992) have shown that the effective Young's modulus of a two-dimensional isotropic medium containing holes (2-D cellular solid) is independent of the Poisson ratio of the

[4] As a comparison, $a=0.12$ for an Na crystal, and $a=1.00$ for a W crystal.

[5] Higher moduli can be obtained from the SC model with different R_1/L. For example, $R_1/L=0.45$ and $v=0.3$ gives $(\bar{E}/E)/(\bar{\rho}/\rho)$ between 0.24 (Reuss) and 0.26 (Voigt) for $(\bar{\rho}/\rho)=0.01$, and $(\bar{E}/E)/(\bar{\rho}/\rho)=0.34$ (Reuss and Voigt) for $(\bar{\rho}/\rho)=0.1$. If the spheres are further 'inflated', the SC model approaches the box model, for which $(\bar{E}/E)/(\bar{\rho}/\rho)$ is between 0.43 (Reuss) and 0.50 (Voigt) for $v=0.3$.

isotropic matrix material. Similar results for 3-D cellular solids are not known to the author. It is interesting to note that the effective Young's modulus increases by approximately 25% for the BCC and FCC models when Poisson's ratio decreases from 0.45–0, see Tables 4 and 5 where the effects of Poisson's ratio of the cell walls on effective properties are given. The 'plane strain' modulus $E/(1-v^2)$ is also affected but to a lesser extent, approximately 13% for the same models and range of Poisson's ratio.

7. Experimentally measured elastic moduli of metal and polymer foams

The experimental data on Divinycell (1995, 1992a, b) H, HT, and HCP grade closed cell polymer foam materials, with absolute densities in the ranges 36–250 kg/m^3 (H-grade), 50–110 kg/m^3 (HT-grade), and 200–400 kg/m^3 (HCP-grade) show a dependence of moduli (Young's modulus E and shear modulus G) which is neither linear nor quadratic. Linear regression ($\log \bar{E}$ and $\log \bar{G}$ vs $\log(\bar{\rho}/\rho)$) give the exponent m in eqn (9) in the range 1.09–1.5 for the H, 0.77–0.94 for the HT, and 1.07–1.46 for the HCP grades. Divinycell (1995, 1992a, b) gives the Poisson ratio $v = 0.32$ for all these materials, independent of density, which means that all moduli (E, G, K) scale in the same way with density. This is not completely consistent with their data but probably a fair approximation. We conclude that these polymer foams scale more or less linearly with density. The quotient $(\bar{E}/E)/(\bar{\rho}/\rho)$ is then of utmost interest.

Assuming Young's modulus $E = 2.5$ GPa and density $\rho = 1400$ kg/m^3 for the cell wall polymer in the Divinycell H-grade foams, the quotient $(\bar{E}/E)/(\bar{\rho}/\rho)$ is in the ranges 0.12–0.58 for H30, 0.17–0.53 for H45, 0.19–0.56 for H60, 0.22–0.60 for H80, 0.27–0.70 for H100, 0.30–0.75 for H130, 0.31–0.81 for H160, 0.34–0.87 for H200, and 0.34–0.90 for H250, where the ranges cover tests performed in different material orientations, and tension and compression. All values were taken from the Divinycell manual (1995). The large ranges are partly due to anisotropy of the foams, and the numbers just given include tests performed both perpendicular and parallel to the plane of the foam sheets (the foams are manufactured in sheets). Compression tests performed in the same material direction but with two different test methods [ASTM D 1621-73 (reapproved 1979) Proc A, and Proc B (old standards)] give values for compressive moduli which for some materials differ by more than a factor of two, Divinycell (1995, 1992a, b).

The quotient $(\bar{E}/E)/(\bar{\rho}/\rho)$ cannot exceed 0.50 for an isotropic foam when $v = 0.3$, see eqn (43). The present assumption for Young's modulus of the cell walls, $E = 2.5$ GPa, may therefore be erroneous. Micro and nano indentations are presently being prepared with the goal to experimentally measure cell wall properties.

The presently produced porous metals are still in an initial stage of development as a structural material, and the properties, normalized with the properties of the cell walls, of the foams are inferior to those of for example polymer foams. The reason for the relatively poor behavior of the metal foams is likely to be found in the micro structure of the metal foams. Figures 9 and 10 show morphologies of the Alporas aluminum foam from Shinko Wire, and the H130 polymer foam from Divinycell. The relative densities are $\bar{\rho}/\rho = 0.081$ for the aluminum foam, and $\bar{\rho}/\rho = 0.093$ for the polymer foam. The relative Young's moduli $\bar{E}/E$ divided by relative densities $\bar{\rho}/\rho$ of these foams are approximately $(\bar{E}/E)/(\bar{\rho}/\rho) = 0.23$ and $(\bar{E}/E)/(\bar{\rho}/\rho) = 0.41$, respectively, assuming Young's modulus $E = 68$ GPa and density $\rho = 2700$ kg/m^3 for the aluminum alloy, Young's

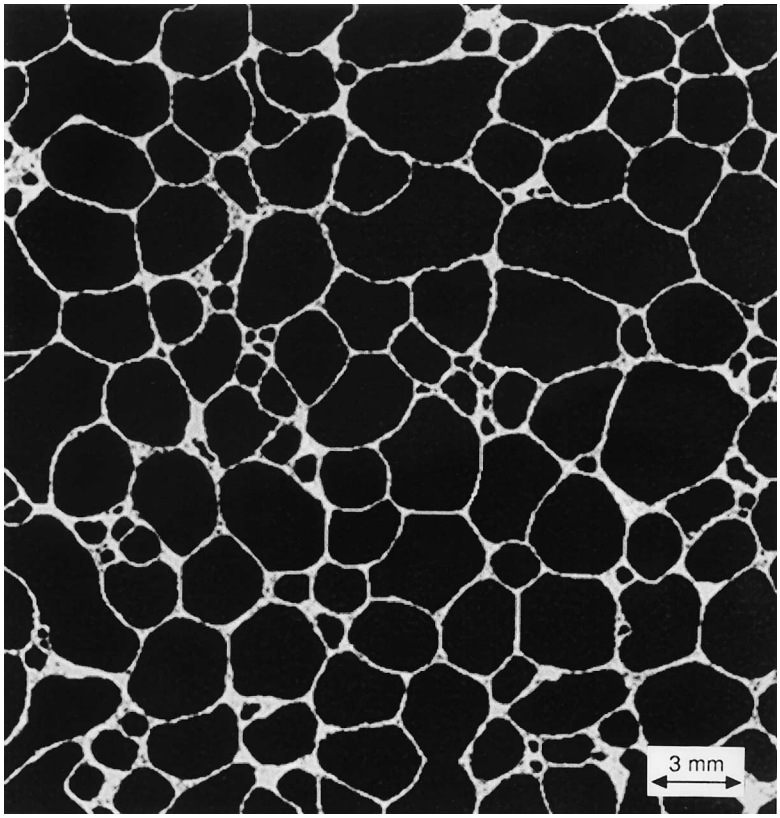

Fig. 9. Morphology of the aluminum closed cell foam Alporas from Shinko Wire. Relative density is $\bar{\rho}/\rho = 220/2700 = 0.081$.

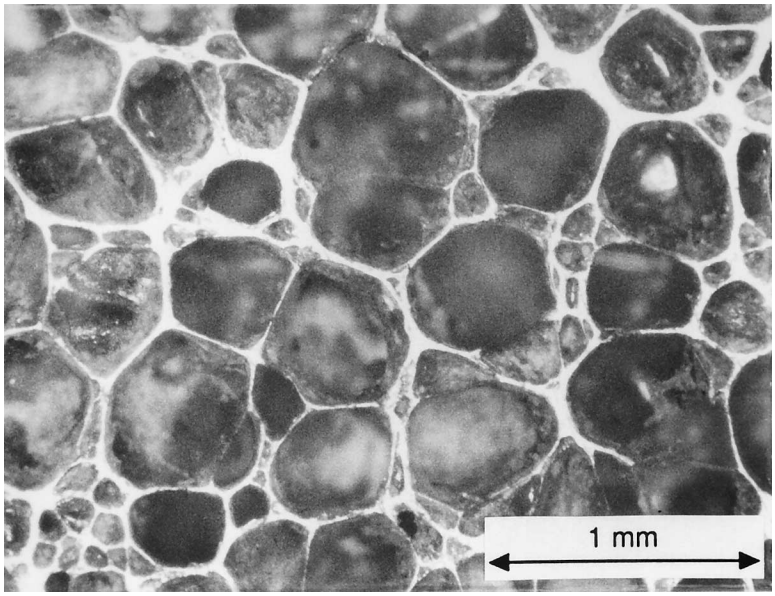

Fig. 10. Morphology of the expanded polymer closed cell foam H130 from Divinycell (1995). Relative density is $\bar{\rho}/\rho = 130/1400 = 0.093$.

modulus $\bar{E} = 1.25$ GPa for the aluminum foam, Young's modulus $E = 2.5$ GPa and density $\rho = 1400$ kg/m^3 for the polymer, and Young's modulus $\bar{E} = 95$ MPa for the polymer foam. The moduli for both foams were measured during unloading, which for the aluminum foams give considerably higher moduli than what is obtained during initial loading when plastic flow likely occurs at stress concentrations. The experimental values of the foams were obtained by Sugimura et al. (1997).

8. Note on scaling of stiffness with density

The scaling of elastic stiffness with relative density was discussed in the beginning of the paper. The FEM models of the foams predict that both Young's and bulk moduli scale linearly with density. Different moduli can scale differently for a given material; an example being the 2-D honeycomb, depicted in Fig. 1, whose 2-D Young's modulus scales cubically and 2-D bulk modulus scales linearly with density. The analytic mono-disperse closed cell simple cubic hollow spheres model predicts some different scalings of bulk modulus with density, but the model is not realistic for the presently considered polymer and aluminum foams.

The Young's modulus is easily measured in a tensile test. The bulk modulus is more difficult to measure, but it can be estimated by assuming isotropy and linear elasticity of the foam and measuring both axial and transverse strain in a (uniaxial) tensile test. If the bulk modulus scales for example linearly with density, $\bar{K} = c_K K(\bar{\rho}/\rho)$, and the Young's modulus quadratically, $\bar{E} = c_E E(\bar{\rho}/\rho)^2$, then Poisson's ratio will for low densities approach 1/2,

$$\bar{\nu} = \frac{3\bar{K} - \bar{E}}{6\bar{K}} = \frac{3c_K K - c_E E(\bar{\rho}/\rho)}{6c_K K} = \frac{1}{2} - \frac{c_E}{c_K}\left(\frac{1}{2} - \nu\right)\left(\frac{\bar{\rho}}{\rho}\right) \to \frac{1}{2} \quad \text{when } \left(\frac{\bar{\rho}}{\rho}\right) \to 0 \tag{44}$$

Gibson and Ashby (1988) indicate that some foams deform locally due to bending in the cell members when the foam is subjected to (macroscopic) deviatoric deformations, and due to stretching in the cell members when the foam is subjected to (macroscopic) isotropic deformations. The 2-D honeycomb is depicted in Fig. 1 has this behavior. However, the closed cell PVC based foams from Divinycell (1995, 1992a, b) behave differently; all foam stiffnesses scale more or less linearly with density, and Poisson's ratio is approximately 0.32 for all the foams, independent of density.

9. Discussion on reasons for deviations between theory and experiments

There are a number of reasons that the elastic properties of the cellular materials differ from the calculated properties. The reason are most likely hidden in the complex geometrical micro structure of the cellular solids, at least as long as the material of the cell wall is not altered during the processing of the foam.

Figures 9 and 10 of the morphologies of the aluminum and polymer foams show that both foams have 'imperfections' such as non-uniform cell size (multi-dispersity). The ratio between

volumes of the largest and smallest cells is as much as two or three orders of magnitude for both materials. Both materials also have non-uniform cell wall thicknesses, where the ratio between thick and thin walls is approximately an order of magnitude. The metal forms have some excess material, which is believed not to contribute to strength or stiffness, at locations where cell walls meet, and collected on cell walls. This excess material may not affect foam properties, but since it increases the weight of the foam, the relative properties are reduced. The major difference between the two materials seems to be the straightness of the cell walls. The cell walls of the aluminum foam are more wavy than those of the polymer foam.

The influence of cell wall waviness on stiffness of cellular solids has been addressed by Grenestedt (1998). The influence is rather large. For example, waviness in the cell walls with an amplitude which is five times the cell wall thickness leads to a stiffness decrease in the order of 40%. The influence of different cell wall thicknesses within a cellular solid has been addressed by Grenestedt and Bassinet (1998). The influence is not as significant. A statistical thickness distribution, where the thickest cell walls were 19 times as thick as the thinnest, results in a 15–20% loss of stiffness as compared with a foam with the same geometry but with all cell walls having the same thickness.

Some further sense for the influence of cell wall curvature can be gained by comparing the elastic response of the simple cubic arrangement of spheres with the Kelvin BCC structure. The bulk moduli of the analytic sphere models scale linearly with density for very low relative densities when the contact area between neighboring spheres is finite, but quadratically for higher densities. The FEM analysis of the SC sphere model with large contact regions showed a more or less linear scaling, and that the sphere model is more compliant than the BCC model for all densities The FEM sphere model and the BCC model are qualitative not too different, except that the former has a lot of curvature in the cell walls whereas the latter consists of only flat cell walls. The BCC model is approximately twice as stiff as the SC model with $R_1/L = 1/4$ (see Tables 1 and 2).

Regarding the influence of cell size distribution, the mono-disperse Kelvin BCC may be compared to the bi-disperse FCC structure. These two structures have virtually identical elastic properties, independent of both relative densities and base material properties (Poisson's ratio). This fact is naturally far from sufficient to draw any major conclusions about the effect of multi-dispersity, but it indicates that the effect may be small.

10. Summary and conclusions

A number of models for cellular solids were presented, and the foam properties these models predict were calculated and compared.

Two flat faced models, denoted BCC and FCC, are believed to be quite realistic models for actual closed cell foams. The effective Young's moduli predicted by these models scale linearly with density of the cellular material, which conforms well with experimental data from for example expanded PVC based foams. Both models predict the Poisson ratio $\bar{\nu} = 0.32$ for the foams when $\nu = 0.3$ for the cell wall material; this is identical to what Divinycell (1995, 1992a, b) reports. Quantitatively, the agreement with experimental data for the PVC based foams is good, whereas it is off by approximately a factor of two for aluminum foam.

Acknowledgements

This work was performed during my sabbatical to Harvard University, Division of Engineering and Applied Sciences. The immense stimulation I received from Profs John W. Hutchinson, Bernard Budiansky and Anthony G. Evans is gratefully acknowledged. Dr Yuki Sugimura is gratefully acknowledged for providing experimental results.

Appendix A: Equivalent isotropic stiffnesses obtained from cubic stiffnesses

Many of the real foams which we wish to model are more or less isotropic. From the results from the calculations on the cubic cell models, we therefore may wish to create an 'equivalent' isotropic medium, whose stiffnesses are given for example by shear modulus $\bar{G}$ and bulk modulus $\bar{K}$. This can be done for example by assuming that the foam looks like a polycrystal as depicted in Fig. A1, i.e. the foam consists of 'grains' with cubic symmetry which are large compared to the individual cells. There are many grains in an RVE of the foam, arranged in different orientations, such that the RVE is essentially isotropic. In general, the stress and deformation states within the grains are complex, but bounds on the isotropic stiffnesses $\bar{G}$ and $\bar{K}$ can easily be obtained by assuming simple deformation or stress fields throughout the RVE. For the sake of completeness, some of the results are re-derived here.

Upper bound stiffnesses can be obtained by assuming that the strain in each point in the RVE is the same. This was done by Voigt (1928). The index 'V' is used for quantities which are related to the Voigt bound. A constant strain state is a kinematically feasible strain field when the boundaries are displaced in agreement with a homogeneous strain state, and the resulting strain energy will due to the minimum of the potential energy be an upper bound on the strain energy in the RVE (the potential energy equals the strain energy since the only loading is boundary displacements). With V^r denoting the volume of grain r, and $\bar{C}^{cub,r}_{ijkl}$ the cubic stiffness components of grain r expressed in a global coordinate system, the upper bound strain energy density in the RVE is

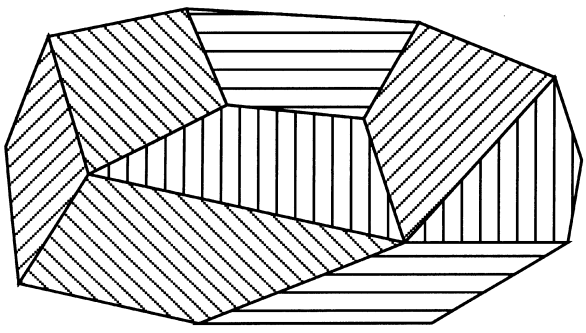

Fig. A1. A model for an isotropic foam, consisting of 'grains' made of cellular solid with cubic symmetry. Each grain is large compared to the cell size of the cellular solid from which it is made.

$$\bar{W}^V = \frac{\sum_r (V^r \bar{C}^{cub,r}_{ijkl} \bar{\varepsilon}_{ij} \bar{\varepsilon}_{kl})}{2\sum_r V^r} = \frac{\bar{\varepsilon}_{ij}\bar{\varepsilon}_{kl} \sum_r (V^r \bar{C}^{cub,r}_{ijkl})}{2\sum_r V^r} \tag{A1}$$

By equating this expression to the strain energy in eqn (2) in the main body of the paper, the foam stiffnesses are obtained

$$\bar{C}^V_{ijkl} = \frac{\sum_r (V^r \bar{C}^{cub,r}_{ijkl})}{\sum_r V^r} \tag{A2}$$

This expression can be simplified by using the invariants of the stiffness tensors ($\bar{C}^{cub,r}_{ijkl}$ depends on the orientation of grain r, whereas the invariants $\bar{C}^{cub,r}_{iijj}$ and $\bar{C}^{cub,r}_{ijij}$ do not),

$$\begin{aligned} \bar{C}^V_{iijj} &= \bar{C}^{cub}_{iijj} \\ \bar{C}^V_{ijij} &= \bar{C}^{cub}_{ijij} \end{aligned} \tag{A3}$$

where the index 'r' was removed since the stiffness invariants are the same for all grains. The isotropic upper bound stiffnesses are

$$\begin{aligned} \bar{K}^V &= \bar{C}^V_{iijj}/9 \\ \bar{G}^V &= (3\bar{C}^V_{ijij} - \bar{C}^V_{iijj})/30 \end{aligned} \tag{A4}$$

These are upper bounds on $\bar{K}$ and $\bar{G}$, which is seen by for example, making use of the strain state $\bar{\varepsilon}_{12} = 1/\sqrt{2}$, other $\bar{\varepsilon}_{ij} = 0$, which gives $\bar{G}^V = \bar{W}^V \geqslant \bar{W} = \bar{G}$, and $\bar{\varepsilon}_{ij} = \sqrt{2}/3\delta_{ij}$, which gives $\bar{K}^V = \bar{W}^V \geqslant \bar{W} = \bar{K}$ (recall that the foam is isotropic).

Lower bound stiffnesses for a polycrystal can similarly be obtained by assuming that the stress in each point in the RVE is the same, as was done by Reuss (1929), and using the minimum of the complimentary potential energy. The index 'R' is used for quantities which are related to the Reuss bound. It is essential for these lower bounds that the micro structure is as described, i.e. there are grains with known properties which are so large compared to the individual cells that they can be considered to be homogeneous, and there are many grains in an RVE of the foam. Under completely general circumstances, the lower bound stiffnesses are zero (which is obtained when cell walls are not connected).

The result from the lower bound analysis is that the invariants of the foam and grain compliancies are equal,

$$\begin{aligned} \bar{S}^R_{iijj} &= \bar{S}^{cub}_{iijj} \\ \bar{S}^R_{ijij} &= \bar{S}^{cub}_{ijij} \end{aligned} \tag{A5}$$

and the lower bound stiffnesses are

$$\bar{K}^R = \frac{1}{\bar{S}^R_{iijj}}$$

$$\bar{G}^R = \frac{15}{2(3\bar{S}^R_{ijij} - \bar{S}^R_{iijj})} \tag{A6}$$

When the grains have cubic symmetry, these upper and lower bounds on bulk modulus coincide. This does not imply that we can accurately determine the bulk modulus for the real foam, but only for the polycrystal model considered here.

Better bounds for a polycrystal consisting of cubic crystals can be obtained by the method of Hashin and Shtrikman (1962). Other estimates for the shear modulus can be obtained by using self consistent models (without bounding properties), as done by e.g. Hershey and Dahlgren (1954) and Kröner (1958). We refer to these papers for further discussions.

Appendix B: Deformation of a spherical cap

Reissner (1946a, b) has given expressions for deformations of spherical caps using shallow shell theory with Love–Kirchhoff kinematics. In the case of an evenly distributed load within a circular region of radius r_p on the spherical cap, whose curvature is R and wall thickness t, the center deformation is

$$w_0 = \frac{\sqrt{12(1-\nu^2)}}{\pi}\frac{PR}{Et^2}\left(\frac{\ker'\mu}{\mu} + \frac{1}{\mu^2}\right) \tag{B1}$$

where

$$\mu = \sqrt[4]{12(1-\nu^2)}\frac{r_p}{\sqrt{Rt}} = \sqrt[4]{12(1-\nu^2)}\sqrt{\frac{\pi}{2}}\frac{r_p}{R}\sqrt{\left(\frac{\rho}{\bar{\rho}}\right)} \tag{B2}$$

and E and ν are Young's modulus and Poisson's ratio for the cap material, P is the total force on the circular region, and $\ker'\mu = \mathrm{d}/\mathrm{d}\mu\ \mathrm{Re}\,[K_0(\mu\sqrt{i})]$ where K_0 is a modified Bessel function of the zeroth order. Two extreme cases of interest are the case of point contact ($\mu = 0$), for which

$$w_0 = \frac{\sqrt{3(1-\nu^2)}}{4}\frac{PR}{Et^2} \tag{B3}$$

and the case of vanishing relative density and finite contact area ($\mu = \infty$), for which

$$w_0 = \frac{PR^2}{\pi E t r_p^2} \tag{B4}$$

The effective (average) strain of the cellular solid consisting of hollow spheres is an integral of the displacement over the contact surface between the spheres. For simplicity, but with some loss of accuracy, the effective strain can be approximated as $\bar{\varepsilon}_{11} = w_0/R$, etc., i.e. using the deflection at the center of the contact region rather than the integrated average.

Table B1
Bulk modulus for the cellular solid using the spherical cap approximation. Poisson's ratio is $v = 0.3$. Observe that μ is constant when $(r_p/R)\sqrt{(\rho/\bar{\rho})}$ is constant

$(\bar{\rho}/\rho)$	$\bar{K}/E^{(a)}$ $r_p/R = 0.01$	$\bar{K}/E^{(b)}$ $r_p/R = 0.01$	$\bar{K}/E^{(a)}$ $r_p/R = 0.1$	$\bar{K}/E^{(b)}$ $r_p/R = 0.1$	$\bar{K}/E^{(c)}$ $\mu = 0$ $r_p/R = 0$	$\bar{K}/E^{(d)}$ $\mu = \infty$ $r_p/R = 0.01$	$\bar{K}/E^{(d)}$ $\mu = \infty$ $r_p/R = 0.1$
0.1	8.20×10^{-4}	8.22×10^{-4}	9.52×10^{-4}	1.04×10^{-3}	8.18×10^{-4}	1.67×10^{-6}	1.67×10^{-4}
0.01	8.37×10^{-6}	8.52×10^{-6}	1.87×10^{-5}	2.58×10^{-5}	8.18×10^{-6}	1.67×10^{-7}	1.67×10^{-5}
0.001	9.52×10^{-8}	1.04×10^{-7}	1.67×10^{-6}	1.85×10^{-6}	8.18×10^{-8}	1.67×10^{-8}	1.67×10^{-6}
10^{-4}	1.87×10^{-9}	2.58×10^{-9}	1.67×10^{-7}	1.72×10^{-7}	8.18×10^{-10}	1.67×10^{-9}	1.67×10^{-7}
10^{-5}	1.67×10^{-10}	1.85×10^{-10}	1.67×10^{-8}	1.68×10^{-8}	8.18×10^{-12}	1.67×10^{-10}	1.67×10^{-8}
10^{-6}	1.67×10^{-11}	1.72×10^{-11}	1.67×10^{-9}	1.67×10^{-9}	8.18×10^{-14}	1.67×10^{-11}	1.67×10^{-9}

(a) Effective strain determined by the deflection in the center of the contact area.
(b) Effective strain determined by integrating the deflection over the contact area.
(c) Equation (B7).
(d) Equation (B8).

For a simple cubic arrangement, the effective (average) stress under hydrostatic loading is $\bar{\sigma}_{11} = \bar{\sigma}_{22} = \bar{\sigma}_{33} = P/L^2$ where $L = 2R$ is the length of the cubic unit cell. The relative density is

$$\frac{\bar{\rho}}{\rho} = \frac{\pi}{2}\frac{t}{R} \tag{B5}$$

The effective bulk modulus of the cellular solid with this micro structure, is

$$\bar{K} = \frac{E}{6\pi\sqrt{3(1-v^2)}}\left(\frac{\bar{\rho}}{\rho}\right)^2 \frac{\mu^2}{\mu\,\mathrm{ker}'\,\mu+1} \tag{B6}$$

when $\bar{\varepsilon}_{11} = w_0/R$. The bulk modulus according to eqn (B6) is tabulated in Table B1, together with the bulk modulus which is obtained when the strain is computed by integrating the deflection over the contact region.

Two extreme cases of eqn (B6) are the cases of point contact ($\mu = 0$), for which

$$\bar{K} = \frac{4E}{3\pi^2\sqrt{3(1-v^2)}}\left(\frac{\bar{\rho}}{\rho}\right)^2 \tag{B7}$$

and the case of vanishing relative density and finite area contact ($\mu = \infty$), for which

$$\bar{K} = \frac{E}{6}\left(\frac{\bar{\rho}}{\rho}\right)\left(\frac{r_p}{R}\right)^2 \tag{B8}$$

It can be noted that Poisson's ratio, here defined using contraction in the x_2 and x_3 directions when loaded in the x_1 direction in the way of the uniaxial tensile test, is zero.

References

Born, M., Huang, K., 1954. Dynamical Theory of Crystal Lattices. Oxford University Press, pp. 129–140.
Budiansky, B., 1987. Private communication.
Budiansky, B., 1996. Private communication.
Cherkaev, A.V., Lurie, K.A., Milton, G.W., 1992. Invariant properties of the stress in plane elasticity and equivalence classes of composites. Proceedings of the Royal Society of London A, 438, 519–529.
Christensen, R.M., 1986. Mechanics of low density materials. Journal of the Mechanics and Physics of Solids 34 (6), 563–578.
Christensen, R.M., Waals, F.M., 1972. Effective stiffness of randomly oriented fibre composites. Journal of Composite Materials 6, 518–532.
Divinycell, 1995. Technical Manual H Grade.
Divinycell, 1992a. Technical Manual HT Grade.
Divinycell, 1992b. Technical Manual HCP Grade
Gibson, L.J., Ashby, M.F., 1988. Cellular Solids : Structure and Properties. Pergamon Press.
Grenestedt, J.L., 1998. Influence of wavy imperfections in cell walls on elastic stiffness of cellular solids. Journal of the Mechanics and Physics of Solids 46 (1), 29–50.
Grenestedt, J.L., Bassinet, F., 1998. Influence of cell wall thickness variations on elastic stiffness of closed cell cellular solids, submitted.
Hashin, Z., 1962. The elastic moduli of heterogeneous materials. Journal of Applied Mechanics 29, 143–150.
Hashin, Z., Shtrikman, S., 1962. A variational approach to the theory of the elastic behaviour of polycrystals. Journal of the Mechanics and Physics of Solids 10, 343–352.
Hashin, Z., Shtrikman, S., 1963. A variational approach to the theory of the elastic behaviour of multiphase materials. Journal of the Mechanics and Physics of Solids 11, 127–140.
Hershey, A.V., Dahlgren, V.A., 1954. The elasticity of an isotropic aggregate of anisotropic cubic crystals. Journal of Applied Mechanics, September.
Kröner, E., 1958. Berechnung der elastischen Konstanten des Vielkristalls aus den Konstanten des Einkristalls. Zeitschrift für Physic 151, 504–518.
Matonis, V., 1964. Elastic behavior of low density rigid foams in structural applications. SPE Journal 20, 1024–1030.
Plateau, J.A.F., 1873. Statique Experimentale et Theorique des Liquides Soumis aux Seules Forces Moleculairs. Ghent, Paris, Gauthier-Villars.
Reissner, E., 1946a. Stresses and small displacements of shallow spherical shells. I. Journal of Mathematics and Physics 25, 80–85.
Reissner, E., 1946b. Stresses and small displacements of shallow spherical shells. II. Journal of Mathematics and Physics 25, 279–300.
Reuss, A., 1929. Calculation of flow limits of mixed crystals on the basis of the plasticity of single crystals. Zeitschrift für angewandte Mathematik und Mechanik, 9.
Sugimura, Y., Meyer, J., He, M.Y., Bart-Smith, H., Grenestedt, J., Evans, A.G., 1997. On the Mechanical Performance of Closed Cell A1 Alloy Foams. Acta Mater. 45 (12), 5245–5259.
Thomson, W. (Lord Kelvin), 1887. On the division of space with minimum partitional area. Philosophical Magazine, 24 (151), 503–514.
Voigt, W., 1928. Lehrbuch der Kristallphysik. Teubner, Leipsig, Germany.
Warren, W.E., Kraynik, A.M., 1997. Linear elastic behavior of a low-density Kelvin foam with open cells. Journal of Applied Mechanics 64 (4), 787–794.
Weaire, D., Phelan, R. 1994. A counter-example to Kelvin's conjecture on minimal surfaces. Philosophical Magazine Letters 69 (2), 107–110.